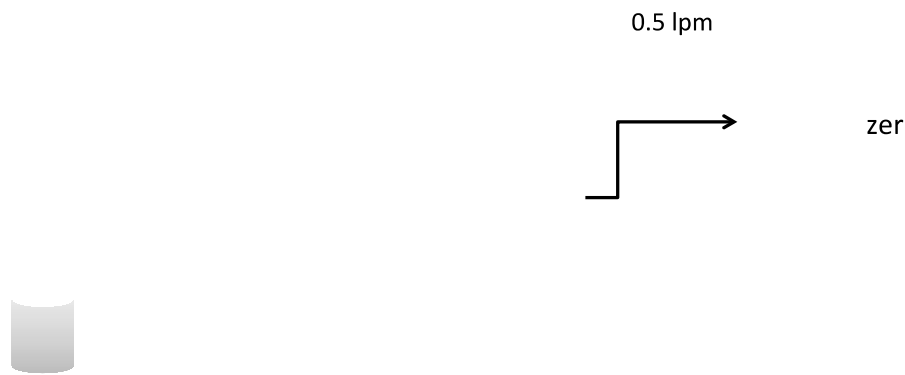


Supplemental Material for Fry, Draper, Barsanti, Smith, Ortega, Winkler, Lawler, Brown, Edwards, Cohen, and Lee, "Secondary organic aerosol formation and organic nitrate yield from NO<sub>3</sub> oxidation of biogenic hydrocarbons."

Contains 8 figures and 2 tables, on 10 pages.

## Supplemental Material

### NCAR Chamber Facility description



**Figure S1.** Schematic of the NCAR environmental chamber facility. Alternating inlet and outlet  $\text{NO}_3$  and  $\text{N}_2\text{O}_5$  measurements are made using two 3-way valves (grey circles). Full instrument names corresponding to acronyms used here are in Table S1.

The NCAR chamber consists of a  $10 \text{ m}^3$  bag made of 0.005 inch thick fluorinated ethylene propylene (FEP) Teflon film suspended in a cubic enclosure. All gaps were sealed to eliminate any light penetration, thus avoiding possible photochemical reactions. Prior to each experiment, the chamber was cleaned using a pulse of ppm-level ozone (20 ppm for  $\sim 5$  minutes) from an electrical discharge ozone generator (Welsbach, Inc.), using pure oxygen to avoid the generation of  $\text{NO}_x$ , followed by 20-30 hours of purified air at a flow of 40 lpm from a zero air generator (Model 737, Aadco Instruments) through HEPA filters (Pall Life Sciences model 12144). The chamber was considered clean after ozone levels had dropped to below 1 ppb, and total particle concentrations were below  $10 \text{ cm}^{-3}$ . Relative humidity was consistently below 5%. Ammonium sulfate seed aerosol was added during one experiment, generated from a 0.1 g/L aqueous solution of ammonium sulfate using an atomizer followed by a diffusion drier, resulting in polydisperse dry ammonium sulfate seed with mode diameter of 40 nm. All flows into and out of the chamber were through 22.2 mm inner diameter stainless steel tubes, which penetrated the chamber through compression fittings. For these experiments, the chamber was run in flow-through mode with a total input flow rate of 40 lpm zero air with slight positive pressure (1-2 mm  $\text{H}_2\text{O}$ ). Gas-phase and aerosol-phase measurements were extracted from the chamber on the wall opposite to the zero air and reactant inputs.

Each experiment was initiated by filling the chamber with the  $\text{NO}_3 + \text{N}_2\text{O}_5$  oxidant at the desired concentration (nominally either 10 ppb or 50 ppb). An  $\text{N}_2\text{O}_5$  trap source was used in these experiments in order to provide a source of pure  $\text{NO}_3$  oxidant with no  $\text{O}_3$ . A calibrated concentration was provided by flowing approximately  $20\text{-}200 \text{ mL min}^{-1}$  of

zero air through a trap containing  $N_2O_5$  crystals, submerged in an isopropyl alcohol and dry ice bath held at a temperature of  $-65$  to  $-60^\circ C$ . The temperature settings depended upon daily trap condition, so before each experiment, flows and temperatures were tuned to achieve the desired  $N_2O_5$  concentration as measured by cavity ringdown spectroscopy (CRDS) and then kept constant for the remainder of that experiment. After  $N_2O_5$  concentrations had reached steady state in the chamber, BVOC was introduced to the inlet flow. In all cases except  $\beta$ -caryophyllene, the BVOC was introduced using a constant flow of a quantified ppm-level gas standard (balance  $N_2$ ) that was subsequently diluted by the 40 liters per minute zero air flow to obtain the desired final chamber concentrations of  $\sim 20$ - $60$  ppb. Cylinder concentrations were verified using a cryo-focused GC-FID system calibrated against a NIST-certified butane/benzene gas standard. In the case of  $\beta$ -caryophyllene, a small flow ( $4$ - $18$  mL/min) of zero air was fed through a heated trap held at  $30$ - $77^\circ C$  containing the liquid hydrocarbon into the chamber input zero air flow. In this case, the  $\beta$ -caryophyllene concentration was verified by sampling  $200$  mL of the BVOC + air mixture onto a two stage adsorbent cartridge (filled with Tenax T and Carbograph B) and analyzed by thermo-desorption GC-MS-FID.

**Table S1.** Instruments used in chamber experiments.

<b>Instrument</b>	<b>Measurement</b>	<b>Flow rate (sampling on INlet or OUTlet flow)</b>	<b>Time resolution</b>
Thermo Scientific chemiluminescence $NO_x$ Analyzer (Model 17i)	$NO$ and $NO_2$	0.6 lpm (OUT)	1 s
2-channel cavity ringdown spectroscopy (CRDS)	$NO_3$ and $N_2O_5$	20-200 mL/min, 0.5 lpm (IN, OUT)	1 s
Ozone monitor (Thermo scientific model 49)	$O_3$	1 lpm (OUT)	1 s
Scanning Mobility Particle Sizer (SMPS)	Particle size distribution (10-350 nm)	0.5 lpm (OUT)	4 min
Thermal Dissociation / Laser Induced Fluorescence	$\Sigma ANs+PNs_{(gas)}$ and $\Sigma ANs+PNs_{(aero)}$	0.5 lpm (OUT)	1 s

## Wall loss analysis

The total chamber flow ( $Q$ ) was 40 liters per minute (or  $0.667 \text{ L s}^{-1}$ ), and the total volume ( $V$ ) was 10,000 L. The resulting  $\beta$  is plotted against particle diameter ( $d_p$ ).

These wall loss rates were used to correct all SMPS data collected during chamber experiments. Size-dependent rates were applied to each raw size distribution to determine the number of particles lost to the walls at each time step. It was assumed that particles were lost to the walls irreversibly and no longer able to act as a gas-condensation reservoir. Thus, to get accurate gross mass yields, these losses were cumulatively added back to the size distributions.

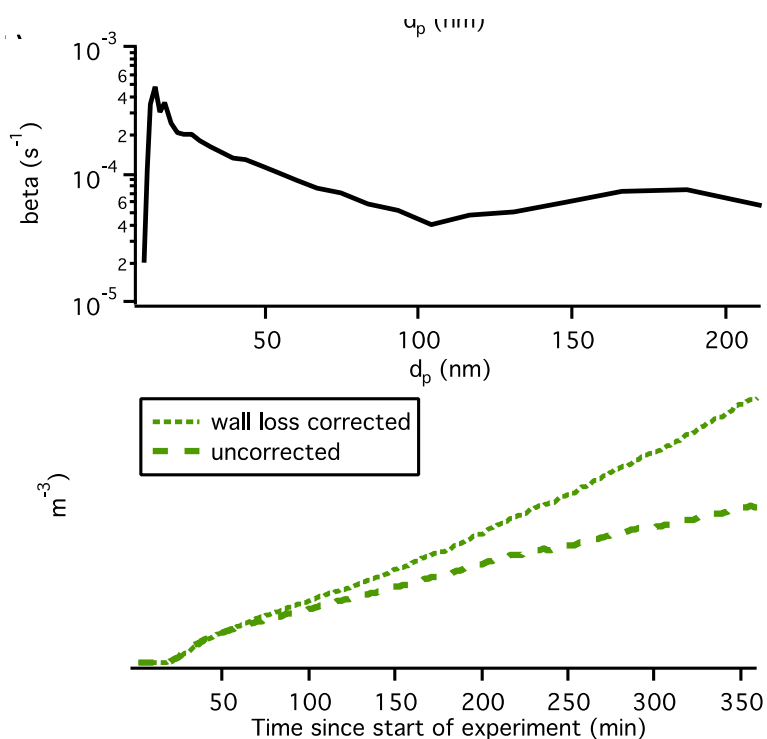


**Figure S2.** Wall loss characterization for the NCAR chamber. (a) Aerosol number size distribution entering (red) and exiting (blue) the chamber at steady state with total flow of 40 lpm, as used in SOA experiments. (b) Calculated values of  $\beta(d_p)$  based on the size distributions shown in 3a and using Eqn. 1. (c) Uncorrected (long dash) and corrected (dotted) mass concentration for the low-concentration  $\beta$ -pinene experiment (Experiment 2), to show magnitude of wall-loss correction.

### Determination of $\Delta VOC$ : method 1: $NO_3$ observation constrained

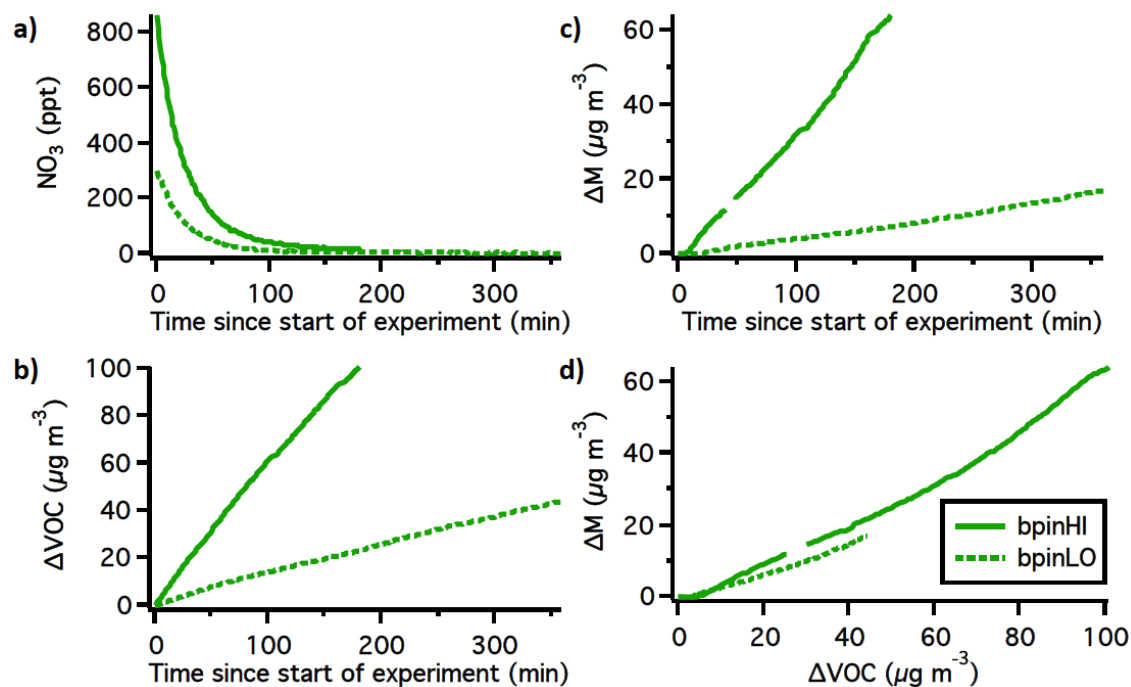


**Figure S3.** Derivation of cumulative  $\beta$ -pinene  $\Delta VOC$  time series for Experiments 2 & 3 (panel b) from  $NO_3$  decay (panel a) and known BVOC addition rate, for the high (solid) and low (dotted) concentration experiments. This is then compared with aerosol mass loading timeseries ( $\Delta M$ ) (panel c), to determine how aerosol mass formed responds to reacted VOC (panel d), from which yields are calculated. Panel d shows the different  $\Delta VOC$  ranges over which the “high” and “low” concentration experiments are run.

## Determination of $\Delta$ VOC: method 2: Model constrained

For this determination of  $\Delta$ VOC, the model (see equation 3 in the main text for general structure) is initiated with an empty chamber.  $\text{N}_2\text{O}_5$  is added for 24 hours to achieve steady-state concentrations matching the initial  $[\text{N}_2\text{O}_5]$  and  $[\text{NO}_3]$  observed for each experiment, using wall loss rate constants that were optimized for the set of all experiments. At hour 24, we begin adding BVOC to the chamber at the rate known from experiment conditions, with continuing addition of  $\text{N}_2\text{O}_5$  at the same rate as previously. The reactions included are shown below, with a table of rate constants. The model is run at 295 K and 0.8 atm (Boulder, CO).

The greatest uncertainty is in the  $\text{RO}_2$  rate constants, for which we followed Ziemann and Atkinson [1] in combination with this useful structure-function relationship page on the MCM: [http://mcm.leeds.ac.uk/MCM/categories/saunders-2003-4\\_6\\_5-gen-master.htm?rxnId=12891](http://mcm.leeds.ac.uk/MCM/categories/saunders-2003-4_6_5-gen-master.htm?rxnId=12891) We assume our  $\text{RO}_2$  radical to all be tertiary, with an enhancement of 2 orders of magnitude due to the beta- $\text{NO}_3$  functional group, which we assume to have the same effect as a beta-hydroxy substitution. We further assume that no  $\text{HO}_2$  will be generated in this system (via  $\text{NO}_3 + \text{RO}_2$  reactions), because the  $\text{RO}_2$  are all tertiary.

Based on our reading of these sources, there appear to be at least 2 orders of magnitude uncertainty in  $\text{RO}_2 + \text{RO}_2$  rate constants, and at least one in  $\text{NO}_3 + \text{RO}_2$ .

1.	$\text{VOC} + \text{NO}_3 \rightarrow \text{RO}_2$	$k_1$
2.	$\text{RO}_2 + \text{NO}_3 \rightarrow \text{products}$	$k_2$
3.	$\text{RO}_2 + \text{RO}_2 \rightarrow \text{products}$	$k_3$
4.	$\text{RO}_2 + \text{NO}_2 \rightarrow \text{RO}_2\text{NO}_2$	$k_4$
5.	$\text{RO}_2\text{NO}_2 \rightarrow \text{RO}_2 + \text{NO}_2$	$k_5$
6.	$\text{NO}_3 + \text{NO}_2 \rightarrow \text{N}_2\text{O}_5$	$k_6$
7.	$\text{N}_2\text{O}_5 \rightarrow \text{NO}_3 + \text{NO}_2$	$k_7$
8.	$\text{N}_2\text{O}_5 \rightarrow \text{walls}$	$k_8$
9.	$\text{NO}_3 \rightarrow \text{walls}$	$k_9$

**Figure S4:** Kinetics box model mechanism.

**Table S2:** Rate constants used in the above model.

Parameter	Value	Source
$k_1$	$\alpha$ -pinene : $6.4 \times 10^{-12} \text{ cm}^3 \text{ molec}^{-1} \text{ s}^{-1}$ $\beta$ -pinene : $2.5 \times 10^{-12} \text{ cm}^3 \text{ molec}^{-1} \text{ s}^{-1}$ $\Delta$ -carene: $9.1 \times 10^{-12} \text{ cm}^3 \text{ molec}^{-1} \text{ s}^{-1}$ limonene : $1.2 \times 10^{-11} \text{ cm}^3 \text{ molec}^{-1} \text{ s}^{-1}$ $\beta$ -caryophyllene : $1.9 \times 10^{-11} \text{ cm}^3 \text{ molec}^{-1} \text{ s}^{-1}$ sabinene : $1.0 \times 10^{-11} \text{ cm}^3 \text{ molec}^{-1} \text{ s}^{-1}$	Calvert, 2000 [2]
$k_2$	$2 \times 10^{-12} \text{ cm}^3 \text{ molec}^{-1} \text{ s}^{-1}$	Vaughan, 2006 [3]
$k_3$	$2 \times 10^{-15} \text{ cm}^3 \text{ molec}^{-1} \text{ s}^{-1}$	Ziemann & Atkinson [1] assuming 100-fold enhancement from beta- $\text{NO}_3$

k <sub>4</sub>	$7.4 \times 10^{-12} \text{ cm}^3 \text{ molec}^{-1} \text{ s}^{-1}$	JPL kinetics eval. 2011
k <sub>5</sub>	$3.3 \text{ s}^{-1}$	JPL kinetics eval. 2011
k <sub>6</sub>	$1.2 \times 10^{-12} \text{ cm}^3 \text{ molec}^{-1} \text{ s}^{-1}$	JPL kinetics eval. 2011
k <sub>7</sub>	$3.2 \times 10^{-2} \text{ s}^{-1}$	JPL kinetics eval. 2011
k <sub>8</sub>	$0 \text{ s}^{-1}$	fit to all model spin-ups
k <sub>9</sub>	$1.5 \times 10^{-3} \text{ s}^{-1}$	fit to all model spin-ups

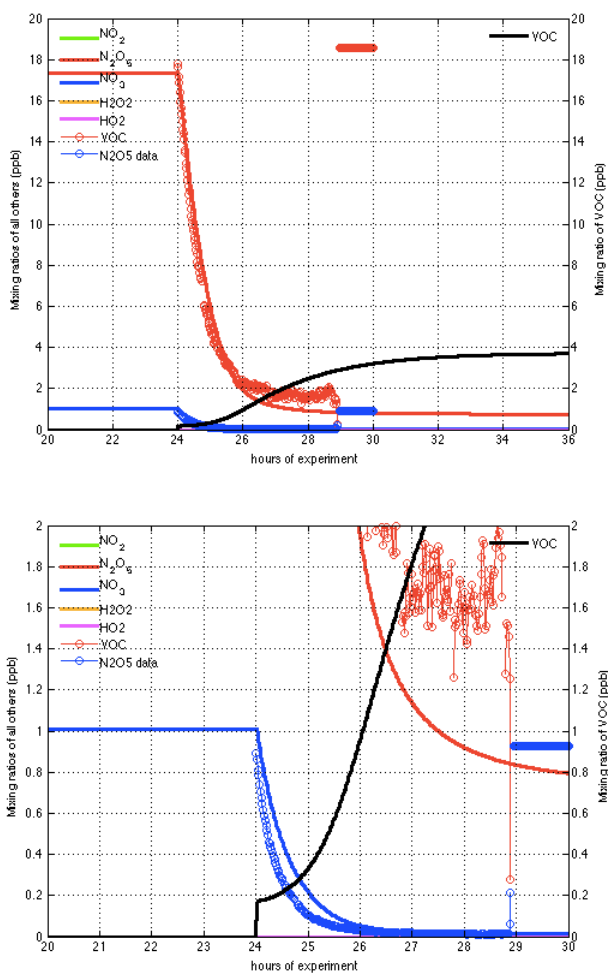


**Figure S5:** Exemplary model run for  $\beta$ -pinene high concentration experiment N2O5 data in red markers, model in red line; NO<sub>3</sub> data in blue markers, model in blue line, and VOC model in black line. There is no HO<sub>2</sub> or H<sub>2</sub>O<sub>2</sub> in these experiments. Lower panel is a zoom-in on upper panel, showing discrepancies in decay timescale of NO<sub>3</sub>/N<sub>2</sub>O<sub>5</sub>. As NO<sub>3</sub> decays, VOC is predicted to build up in the chamber. The cumulative VOC lost to reaction with NO<sub>3</sub> in this model is used as the  $\Delta$ VOC timeseries.

## Molecular structural effects on alkoxy radical fate

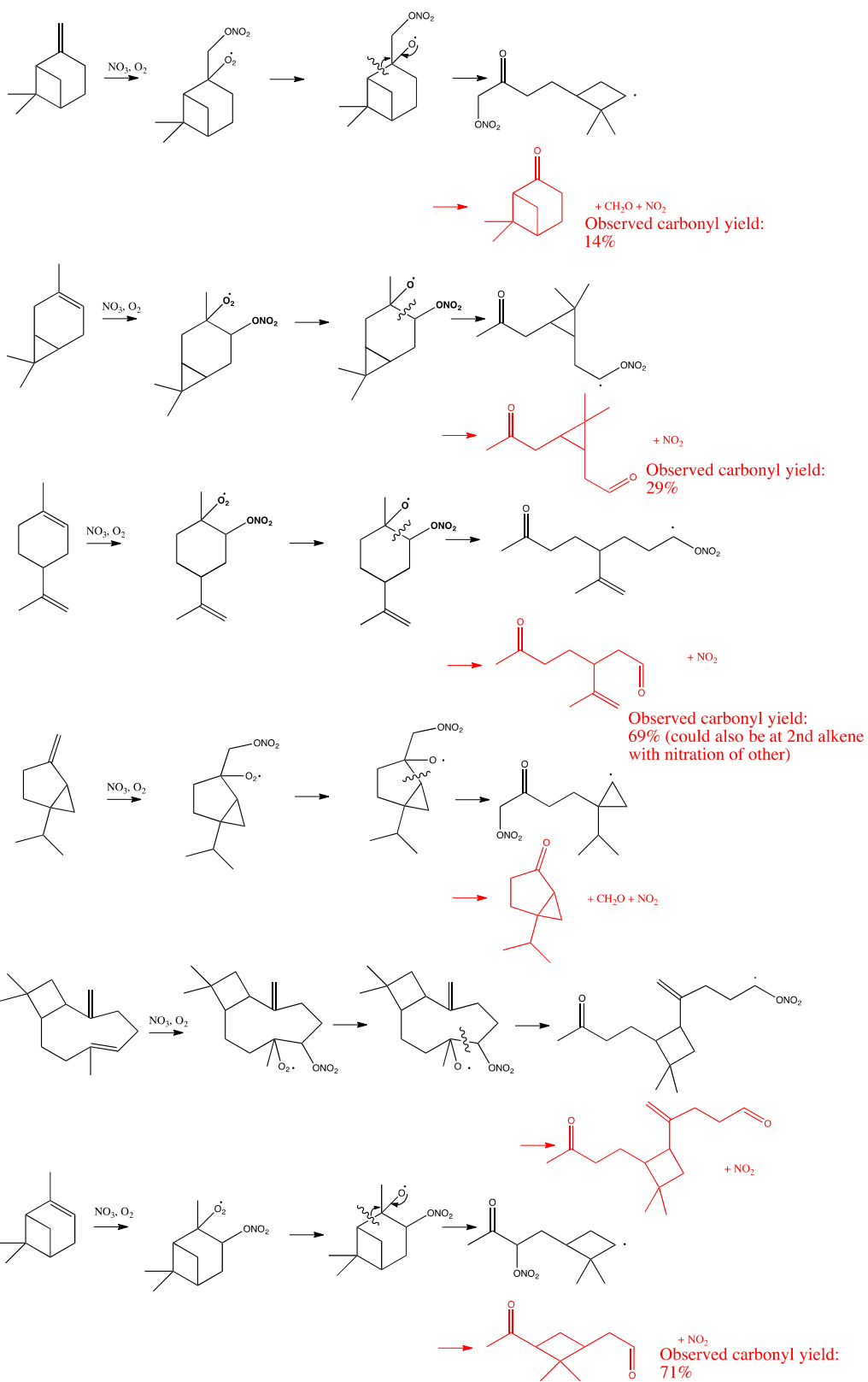




**Figure S6.** Proposed initial steps of nitrate oxidation of (from top to bottom)  $\beta$ -pinene,  $\Delta$ -carene, limonene, sabinene,  $\beta$ -caryophyllene and  $\alpha$ -pinene. Shown in black are the predicted nitrate-carbonyl products based on Vereecken and Peeters [4]; in red are the alternate  $\text{NO}_2$ -shedding dicarbonyl products, with yields reported by Hallquist et al. [5] Note that the carbonyl is not necessarily mutually exclusive with organonitrate formation, especially in the limonene case with two double bonds.

## Organonitrate production

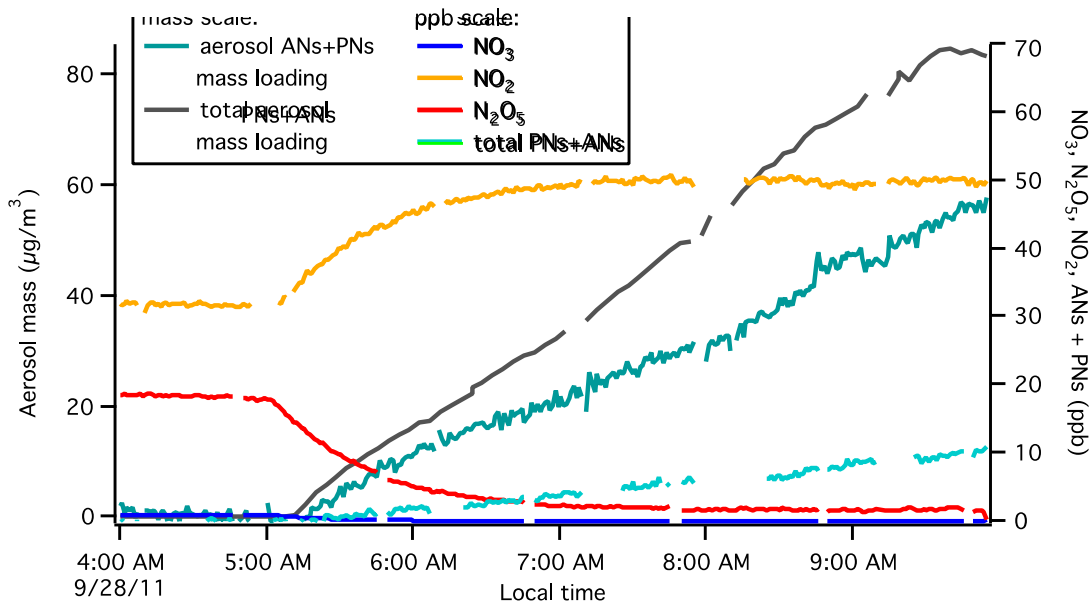
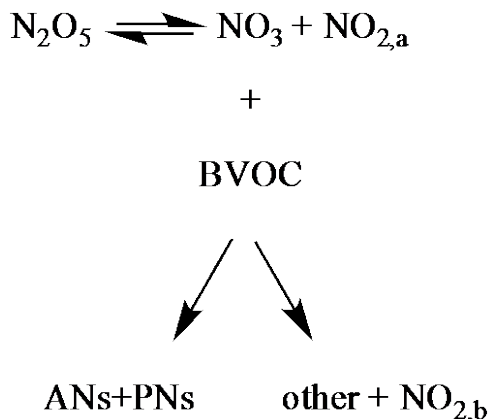


**Figure S7.** Top: Full time series of organonitrate measurements for  $\beta$ -pinene high concentration experiment (#2), in which BVOC was added at 5:20. Bottom: fraction of total aerosol mass that is organonitrate, assuming a mono-nitrate with MW  $\sim 230$  g/mol.

**Figure S8.** Schematic of nitrogen balance, to aid interpretation of Table 3 in the manuscript text.



As reactions proceed, N flows from N<sub>2</sub>O<sub>5</sub> to products:

$$-\Delta[\text{N}_2\text{O}_5] = \Delta[\text{NO}_2]_{\text{a}} + \Delta[\text{ANs+PNs}] + \Delta[\text{NO}_2]_{\text{b}}$$

And the sum of molar NO<sub>2</sub> and ANs+PNs production should equal 2, since each N<sub>2</sub>O<sub>5</sub> precursor contains 2 equivalents N:

$$\frac{\Delta[\text{ANs} + \text{PNs}]}{-\Delta[\text{N}_2\text{O}_5]} + \frac{\Delta[\text{NO}_2]}{-\Delta[\text{N}_2\text{O}_5]} = 2$$

#### References:

1. Ziemann, P. J.; Atkinson, R., Kinetics, products, and mechanisms of secondary organic aerosol formation. *Chemical Society Reviews* **2012**, *41* (19), 6582-6605.
2. Calvert, J. G.; Atkinson, J. A.; Kerr, J. A.; Madronich, S.; Moortgat, G. K.; Wallington, T. J.; Yarwood, G., *Mechanisms of the atmospheric oxidation of the alkenes*. Oxford University Press: New York, NY, 2000.
3. Vaughan, S.; Canosa-Mas, C. E.; Pfrang, C.; Shallcross, D. E.; Watson, L.; Wayne, R. P., Kinetic studies of reactions of the nitrate radical (NO<sub>3</sub>) with peroxy radicals (RO<sub>2</sub>): an indirect source of OH at night? *Physical Chemistry Chemical Physics* **2006**, *8* (32), 3749-3760.
4. Vereecken, L.; Peeters, J., Decomposition of substituted alkoxy radicals-part I: a generalized structure-activity relationship for reaction barrier heights. *Physical Chemistry Chemical Physics* **2009**, *11* (40), 9062-9074.
5. Hallquist, M.; Wangberg, I.; Ljungstrom, E.; Barnes, I.; Becker, K. H., Aerosol and product yields from NO<sub>3</sub> radical-initiated oxidation of selected monoterpenes. *Environ. Sci. Technol.* **1999**, *33* (4), 553-559.